geosciences

MDPI

Article

Challenges Assessing Rock Slope Stability Using the Strength Reduction Method with the Hoek–Brown Criterion on the Example of Vals (Tyrol/Austria)

Mariella Illeditsch [1,2,*], Alexander Preh [1,2] and Johann Thomas Sausgruber [3]

[1] Research Centre of Engineering Geology, Institute of Geotechnics, Vienna University of Technology, 1040 Vienna, Austria; alexander.preh@tuwien.ac.at
[2] pi Geotechnik ZT GmbH, 1140 Vienna, Austria
[3] Federal Ministry Republic of Austria-Agriculture, Regions and Tourism, Department of Forestry and Sustainability, Torrent and Avalanche Control and Protection Forest Policy, 6020 Innsbruck, Austria; thomas.sausgruber@die-wildbach.at
* Correspondence: mariella.illeditsch@tuwien.ac.at

Abstract: To estimate the hazard posed by rock slopes, it is essential to determine the overall stability and potential detachment volume. This is mostly solved using numerical methods together with the strength reduction method (SRM). Many calculation programs do not provide a direct implementation of the Hoek–Brown (HB) criterion. Equivalent Mohr–Coulomb (MC) parameters are often used. Especially for steep rock slopes, the use of equivalent MC parameters with numerical codes and the SRM lead to poor estimates of safety factors. The problem lies in the required and often difficult estimation of a suitable range of minor principal stresses over a 'slope height'. In the example of the stability analysis of the rock slope Vals in Tyrol/Austria, we show the differences between the application of equivalent MC parameters and a direct application of the HB criterion with apparent MC parameters. The detachment volume and stability are overestimated when applying equivalent MC parameters, as confirmed by calculations with the continuum mechanics code FLAC3D (Itasca Consulting Group). However, the SRM with HB material (i.e., apparent MC parameters) results in a safety factor that cannot be applied to HB parameters. To date, it has not been possible to determine the HB parameters for limit equilibrium via the SRM. This challenge was overcome by fitting an HB envelope to the original HB shear envelope reduced by the safety factor. The envelope is adjusted by two HB variables: GSI and D. This allows to determine the HB parameters at limit equilibrium. It helps to make more realistic predictions about the detachment mechanism and volume.

Keywords: rock slopes; rock slope stability; slope stability analysis; strength reduction method; Hoek–Brown criterion; equivalent Mohr–Coulomb parameters

check for updates

Citation: Illeditsch, M.; Preh, A.; Sausgruber, J.T. Challenges Assessing Rock Slope Stability Using the Strength Reduction Method with the Hoek–Brown Criterion on the Example of Vals (Tyrol/Austria). *Geosciences* **2022**, *12*, 255. https://doi.org/10.3390/geosciences12070255

Academic Editors: Hongyuan Liu and Jesus Martinez-Frias

Received: 17 May 2022
Accepted: 14 June 2022
Published: 21 June 2022

1. Introduction

In Vals (Tyrol/Austria), a rock fall with a detachment volume of approximately 117,000 m^3 occurred on 24th December 2017. It destroyed parts of the Valser county road L230 and just missed nearby houses. Mapping and measurements by the Austrian Torrent and Avalanche Control (TAC) after the incident indicate a potentially unstable slope area (Figure 1). This needs to be investigated to predict a possible detachment process and volume in the future.

This was achieved by performing the numerical analysis of the valley flank. Laboratory testing results from the nearby Brenner Basis Tunnel [1] are available. The tunnel is not far from the Vals valley flank and explores the same geological rock units. Thus, the test results are representative for the Vals valley flank. These results and the mapping data (GSI, joint structure) from the TAC are the basis for our numerical analysis.


(**a**) (**b**)

Figure 1. (**a**) Existing scarp and tension crack (red line); and (**b**) tension crack at the top of the potentially unstable area.

We tried to back-calculate the initial wedge failure of the 2017 rock fall event (Figure 2) using the Discrete Element Method DEM (3DEC) and the finite difference method (FDM) (FLAC3D) together with the strength reduction method (SRM) [2]. Different material models were applied. To date, we were not able to recreate this singular event with the models.

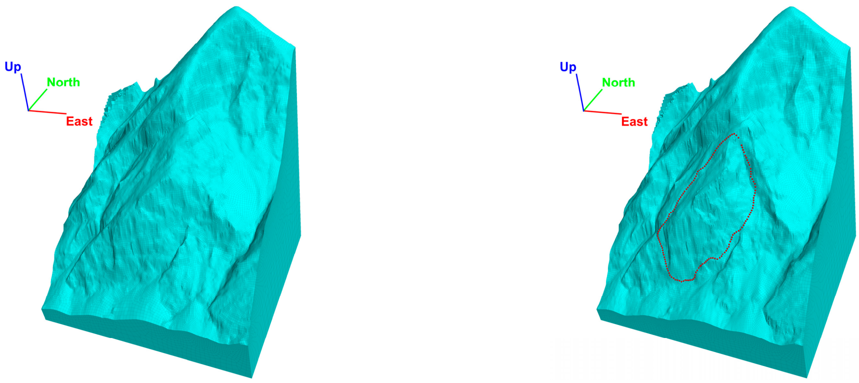

(**a**) (**b**)

Figure 2. FLAC3D model of the Vals valley flank: (**a**) before and (**b**) after the 2017 rock fall event; red: outline of observed moving area.

We used the SRM and Hoek–Brown (HB) material with both equivalent and apparent Mohr–Coulomb (MC) parameters. Our limit equilibrium studies ended up in very different results (refer to Section 6). We describe the implications of these different results and point out the challenge they pose. We propose how to overcome this challenge in this article.

2. Geological Settings

The rock fall event in the valley of Vals (Figure 3) is situated at the Western end of the tectonic Tauern Window. Therein, Penninic metamorphic rock nappe units are currently exposed on the surface. These so-called Bündner Schists build up the valley flanks of Vals [3]. They are composed of graphitic phyllites, calcareous phyllites, and calcareous quartzite bearing schists and marbles. The Bündner Schists represent flyschoid metasediments of the Mesozoic age [4]. These were sedimented in the Valais Ocean [5]. During the Alpine orogeny, the described rocks underwent strong multiphase deformation accompanied by a metamorphism, reaching the green schist facies [6]. Structurally, the Bündner Schists are geologically related to the Glockner Nappe [7]. At the rock face in Vals, the following main sets of discontinuities/faults are present (Figure 4): (1) the persistent but folded rock schistosity (s) dipping 30° to the northwest; (2) NNW–SSE to N–S striking; and

(3) ENE–WSW to E–W striking, inclined joints, and faults. The discontinuity sets (2) and (3) are related to ductile–brittle deformation in the context with Brenner normal fault [8].

Figure 3. Location of Vals in Tyrol/Austria (red circle).

Figure 4. Outcrop, representative for strongly folded and jointed rock mass of Bündner Schists in the valley of Vals: **S**—schistosity (magenta), **2**—conjugate discontinuities (yellow), **3**—fault plane (red).

From a geological point of view, the existing rock mass is inhomogeneous and anisotropic. Soft rocks such as phyllites are intercalated with the hard rocks of calcareous to quartzite-bearing schists and marbles. The uniaxial strength varies from less than 25 MPa to more than 100 MPa. The existing discontinuities are persistent.

On the larger scale, these anisotropic conditions remain the same with depth, so that one can speak of 'homogeneous anisotropy'. To overcome this anisotropy, a continuum mechanical approach was assigned. The rock mass outcrops are described by applying the GSI chart for flysch sediments [9]. According to that, the rock mass in Vals represents a GSI in the range between 32 and 36.

3. Applied Known Methods and Facts

3.1. The Strength Reduction Method (SRM) in FLAC3D

The finite-difference continuum-mechanic program FLAC3D (Itasca Consulting Group) provides the possibility to calculate safety factors by applying the SRM [2]. In this process, the shear strength of the material is gradually reduced to bring the slope to a state of limit equilibrium. The SRM was used in the context of MC materials and the simultaneous reduction in cohesion c and friction angle φ. The factor F is defined according to the following equations:

$$c^{red} = \frac{c}{F} \tag{1}$$

$$\varphi^{red} = arctan\left(\frac{tan\ \varphi}{F}\right) \tag{2}$$

By applying the SRM to the HB criterion, FLAC3D locally approximates the HB parameters by a MC criterion:

$$\tau = \sigma' \cdot \tan \varphi_c + c_c \tag{3}$$

Calculating the apparent cohesion c_c and apparent friction angle φ_c in each zone (depending on σ_3):

$$\varphi_c = 2 \cdot \tan^{-1} \cdot \sqrt{N_{\varphi_c}} - 90 \tag{4}$$

$$c_c = \frac{\sigma_c^{UCS}}{2 \cdot \sqrt{N_{\varphi_c}}} \tag{5}$$

where, for compressive stresses ($\sigma_3 > 0$):

$$N_{\varphi_c} = 1 + a \cdot m_b \cdot \left(m_b \cdot \frac{\sigma_3}{\sigma_{ci}} + s \right)^{a-1} \tag{6}$$

$$\sigma_c^{UCS} = \sigma_3 \cdot (1 - N_{\varphi_c}) + \sigma_{ci} \cdot \left(m_b \cdot \frac{\sigma_3}{\sigma_{ci}} + s \right)^{a} \tag{7}$$

Additionally, for tensile stresses ($\sigma_3 < 0$):

$$N_{\varphi_c} = 1 + a \cdot m_b \cdot (s)^{a-1} \tag{8}$$

$$\sigma_c^{UCS} = \sigma_{ci} \cdot (s)^{a} \tag{9}$$

where σ_{ci} is the unconfined compression strength and m_b, s, and a are HB parameters (see Equations (11)–(13) below) [10].

3.2. Apparent and Equivalent Mohr–Coulomb Parameters

Limit equilibrium can be determined using the MC or the HB criterion. Using the MC criterion, (equivalent) strength parameters c and φ are assumed to be constant for the considered homogenous region. Using the HB criterion, apparent MC parameters (c_c and φ_c) are determined for each individual numerical zone (with variable σ_3). They are thus to be regarded as 'local' parameters, i.e., different in every zone, depending on σ_3 (Figure 5).

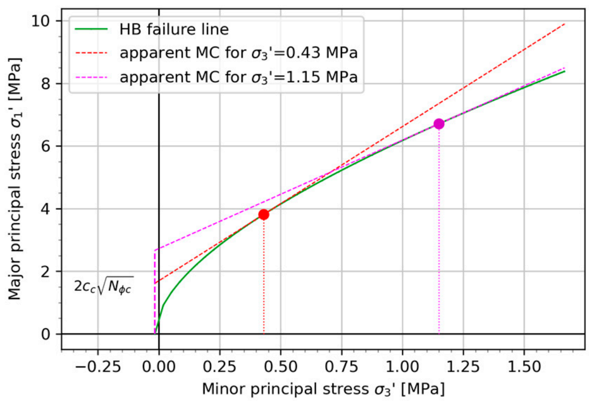

Figure 5. HB failure criterion and its MC approximation with apparent ('local') MC parameters (at two locations).

The advantage of 'local' over equivalent MC parameters has already been demonstrated in the literature. Ref. [11] studied the accuracy of using equivalent MC parameters to estimate the factor of safety. Especially for steep slopes, it leads to poor estimates of safety factors and poor predictions of detachment volumes. The problem lies in the required estimation of a suitable range for smaller principal stresses (σ_3) over the 'slope height' (or 'tunnel depth').

Figure 6 shows the HB criterion and equivalent MC envelope. The equivalent MC envelope is one straight line for the entire homogenous region. It cannot fit the HB curve equally well at all depths (i.e., for all σ_3). For lower and higher σ_3 ranges (regions 1 and 3), equivalent MC parameters may overestimate the ultimate shear strength compared to the HB curve.

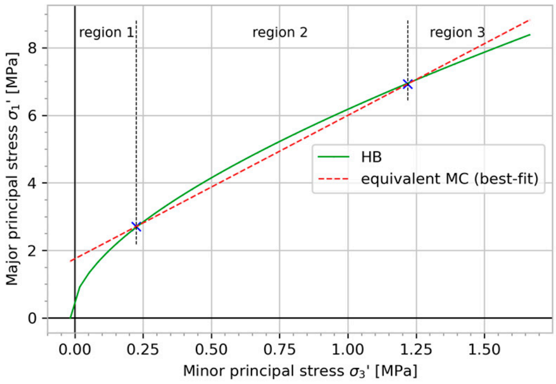

Figure 6. Hoek–Brown criterion and equivalent Mohr–Coulomb envelope.

3.3. Construction of the HB Limit Equilibrium Envelope for a Given Reduction Factor F

The generalized HB criterion [12] for rock masses is nonlinear. This defines the material strength in terms of major and minor principal stresses through the equation

$$\sigma_1 = \sigma_3 + \sigma_{ci} \cdot \left(m_b \cdot \frac{\sigma_3}{\sigma_{ci}} + s \right)^a, \tag{10}$$

where σ_{ci} is the uniaxial compressive strength of the intact rock material, while

$$m_b = m_i \cdot exp\left(\frac{GSI - 100}{28 - 14 \cdot D} \right), \tag{11}$$

$$s = exp\left(\frac{GSI - 100}{9 - 3 \cdot D} \right) \ and \tag{12}$$

$$a = \frac{1}{2} + \frac{1}{6} \cdot \left(e^{-\frac{GSI}{15}} - e^{-\frac{20}{3}} \right), \tag{13}$$

where m_i is an intact rock material property, GSI is the geological strength index, and D is the disturbance factor.

Ref. [13] developed relationships between the shear-normal stress and the principal stress envelopes. The normal and shear stress pair corresponding to a point on a principal stress envelope is given by the following equations:

$$\sigma_n = \frac{1}{2} \cdot (\sigma_1 + \sigma_3) - \frac{1}{2} \cdot (\sigma_1 - \sigma_3) \cdot \frac{\frac{d\sigma_1}{d\sigma_3} - 1}{\frac{d\sigma_1}{d\sigma_3} + 1}, \tag{14}$$

$$\tau = (\sigma_1 - \sigma_3) \cdot \frac{\sqrt{\frac{d\sigma_1}{d\sigma_3}}}{\frac{d\sigma_1}{d\sigma_3} + 1}. \tag{15}$$

For the generalized HB criterion, the following equations relate σ_n and τ to σ_1 and σ_3 [14]:

$$\sigma_n = \frac{1}{2} \cdot (\sigma_1 + \sigma_3) - \frac{1}{2} \cdot (\sigma_1 - \sigma_3) \cdot \frac{a \cdot m_b \cdot \left(m_b \cdot \frac{\sigma_3}{\sigma_{ci}} + s \right)^{a-1}}{2 + a \cdot m_b \cdot \left(m_b \cdot \frac{\sigma_3}{\sigma_{ci}} + s \right)^{a-1}}, \tag{16}$$

$$\tau = (\sigma_1 - \sigma_3) \cdot \frac{\sqrt{1 + a \cdot m_b \cdot \left(m_b \cdot \frac{\sigma_3}{\sigma_{ci}} + s\right)^{a-1}}}{2 + a \cdot m_b \cdot \left(m_b \cdot \frac{\sigma_3}{\sigma_{ci}} + s\right)^{a-1}}. \tag{17}$$

First, the in situ state of the model is calculated. Then, the limit equilibrium routine in FLAC3D ('model factor-of-safety') gradually reduces the apparent ('local') MC parameters φ_c and c_c. Limit equilibrium is reached at the first unstable system state (F_{unstable}). F_{stable} is the safety factor of the last stable system state.

The failure line for a given reduction factor F can be calculated using the following formula:

$$\tau^{red} = \frac{\tau}{F}. \tag{18}$$

The geometric interpretation of lowering an HB shear envelope by a factor F is shown in Figure 7.

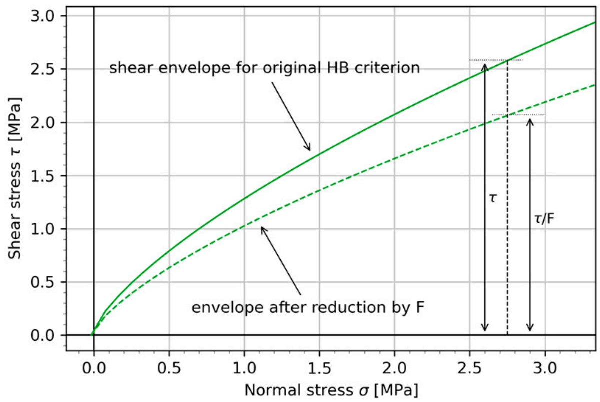

Figure 7. A generalized HB envelope drawn in normal-shear stress space (green), and the resulting envelope after reduction by a factor F (green-dot).

4. The Challenge

The SRM was applied to an MC material model, with MC parameters equivalent to the HB parameters (i.e., equivalent MC parameters). We investigated how different slope heights for calculating the equivalent MC parameters affect the calculation results. What [11] found (see Section 3.2) was confirmed by our calculations. The models show excessively large unstable areas, which cannot be observed in nature (see Section 6.2).

Thus, the HB criterion was used to determine the limit equilibrium using the SRM (see Section 6.3). However, the SRM with HB material requires a local approximation using the MC criterion (apparent MC parameters, see Section 3.1). The reduction factor F calculated in this way cannot be directly used to calculate the HB parameters for the limit equilibrium state.

The SRM leads to a model with chaotically distributed MC parameters in numerical zones (Figure 8). It does not lead to HB parameters for the entire homogeneous area of the model. However, they are required for prediction calculations. The challenge is to find those HB parameters which lead to the chaotic distributions of apparent MC parameters, as shown in Figure 8. In other words, the challenge is to find the HB parameters of the HB envelope for the limit equilibrium state derived via SRM.

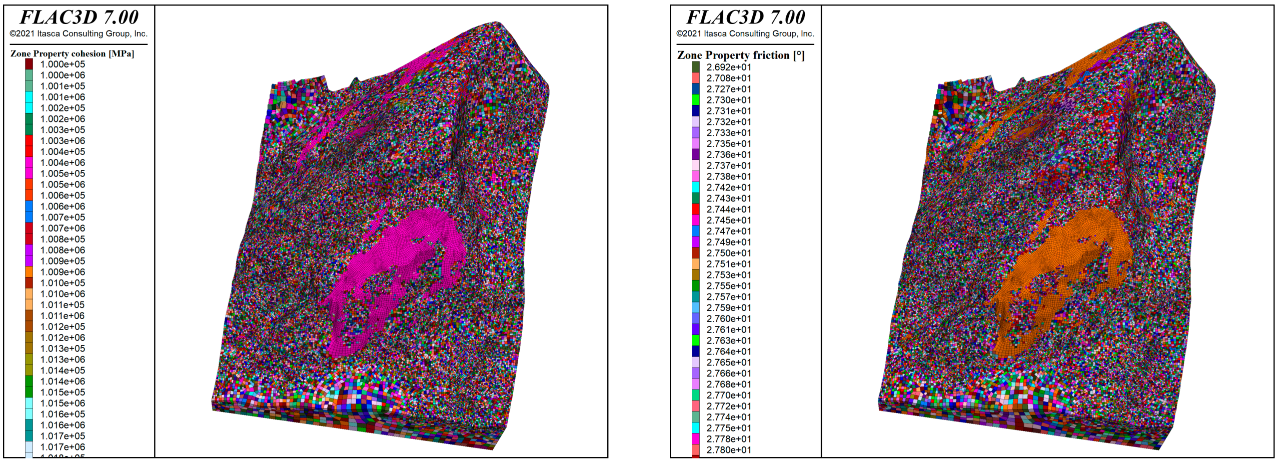

(**a**) (**b**)

Figure 8. Volume model of chaotically distributed (**a**) cohesion and (**b**) friction parameters.

5. Method to Overcome the Challenge: Deriving the HB Parameters Close to the Limit Equilibrium Envelope by Varying GSI and/or D

The reduction factor F cannot be applied to the original HB parameters (as discussed in Section 4).

We need to determine an HB material equivalent to the HB envelope at limit equilibrium state (i.e., reduced by F). This is achieved by adjusting the geological strength index GSI and/or the disturbance Factor D. It is plausible to adjust those parameters due to the following considerations: (1) Based on the statement in Hoek's GSI chart [9], it is more realistic to consider a range of the GSI, rather than a single value; and (2) Since it can be assumed that the rock mass has been disturbed by previous slope movements, the disturbance factor may be increased.

The laboratory parameters m_i, $\sigma_{ci,}$ and E_i are kept constant.

Figure 9 shows the HB envelopes for the in situ state (green), for the limit equilibrium state (green-dot), and for the HB envelope adjusted to the limit equilibrium state by GSI and/or D (yellow).

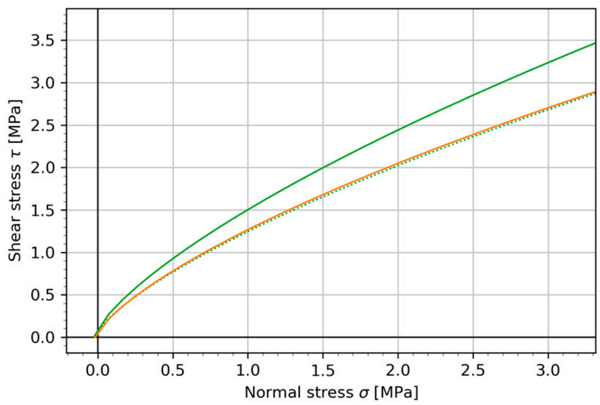

Figure 9. HB failure envelopes in normal-shear stress space; green: in situ state, green-dot: limit equilibrium state, yellow: adjusted to the limit equilibrium state by reducing GSI and/or increasing D.

Since this is an approximation, the derived values of GSI and D should be optimized. We used a concordance check according to [15] to calibrate our model. This is further described in Section 6.4.

6. Stability Analysis of the Valley Flank Vals

We first used the Discrete Element Method DEM (3DEC) for a discontinuum mechanical limit equilibrium study. This failed because of the model size, which required an excessively long computation time. The model size must be sufficiently large to eliminate the possible effects of boundary conditions. Additionally, the results should be meaningful. The dimensions of the model for the Vals valley flank were set at 560 m wide, 400 m deep, and 510 m high. With such a model size, only large simplifications of the joint system would lead to an acceptable computation time (e.g., increasing the joint spacing).

The continuum mechanical finite difference method (FDM) (FLAC3D) achieves calculations of this model size (654,263 zones and 368,552 grid points) within an acceptable computation time. All results presented in this article were derived via FLAC3D.

6.1. Model Procedure

The distance from the area of interest to the edge of the model was chosen so that the boundary conditions had no influence on the behavior of the model. The side faces were fixed in normal direction and the base surface in x, y, and - directions. The in situ stresses were calculated in two steps. In the first step, a purely elastic material behavior was assumed. Plastic deformations were prevented by setting high rock strengths. In the second step, the actual strength values of the material (Table 1) were assigned and the stress state calculated.

Table 1. HB, laboratory, and equivalent MC parameters used for the different limit equilibrium calculations.

State	Initial (Before and After)	Limit Equilibrium		
		Before	After	After Best Fit
Model 1: Equivalent MC Parameters				
φ	42	32.4	31.5	
c (MPa)	0.5	0.353	0.340	
σ_t (MPa)	0.026	0.026	0.026	
$F_{unstable}$		1.420	1.473	
Model 2: Laboratory and HB Parameters				
σ_{ci} (MPa)	45.8	45.8	45.8	45.8
E_i (MPa)	30,000	30,000	30,000	30,000
γ (MN/m3)	0.02728	0.02728	0.02728	0.02728
GSI	34	34	34	34
D	0	0.37	0.37	0.35
m_i	12	12	12	12
m_b	1.14	0.6654491	0.6654491	0.6891914
s	6.53×10^{-4}	2.329×10^{-4}	2.329×10^{-4}	2.480×10^{-4}
a	0.52	0.5170641	0.5170641	0.5170641
$F_{unstable}$		1.207	1.211	

Laboratory testing results [1] and mapping data from the TAC delivered the parameters listed in Table 1. The equivalent MC parameters were determined using the RocData program from [16]. For this purpose, the stress state in the failure surface of the slope movement (shear zone) must be estimated by specifying a ‘slope height’. The slope height related to a possible slope movement was estimated with 80 m. A study of different slope heights was conducted (refer to Section 6.4.1).

The model parameters were applied to the entire model. Thus, each respective model was considered a homogeneous region regarding its rock properties. The limit equilibrium (safety factor) was determined for four different models using the SRM (as described in Section 3.1). The four different models are:

- Model 1a: Mohr–Coulomb before the rock fall event 2017;
- Model 1b: Mohr–Coulomb after the rock fall event 2017;
- Model 2a: Hoek–Brown before the rock fall event 2017; and
- Model 2b: Hoek–Brown after the rock fall event 2017.

6.2. Model 1—Mohr–Coulomb

For model 1, the parameters are listed in Table 1, in the column 'Initial (Before and After)'. The analysis of the valley flank was performed using the MC material model and MC parameters equivalent to the HB parameters.

For the terrain before the rock fall event 2017 (model geometry 'Before'), the reduction factor F_{stable} of the last stable state was 1.418. The reduction factor $F_{unstable}$ of the first unstable state was 1.420. The safety factor can thus be given as 1.42. Applying Equations (1) and (2) gives the MC parameters c = 0.353 MPa and φ = 32.4° at a limit equilibrium.

For the terrain after the rock fall event 2017 (model geometry 'After'), the reduction factor F_{stable} of the last stable state is 1.470. The reduction factor $F_{unstable}$ of the first unstable state is 1.473. The safety factor can thus be given as 1.47. Applying Equations (1) and (2) gives the MC parameters c = 0.340 MPa and φ = 31.5° at the limit equilibrium state.

Comparison of 'Before' and 'After' MC Model

Both model calculations show much larger extents of the moving area than observed. This applies especially to the west and above the observed tension crack. The failure mechanism close to the limit equilibrium state is that of slope creep [17]. This means the continuous decrease in displacements with depth (Figure 10c). A continuous shear band (Figure 10b) separates the moving from the non-moving area (subtype block slope creep, [18]). Due to the extent and depth of the separating shear band (Figure 10a), the movement can be classified as that of a deep-seated landslide.

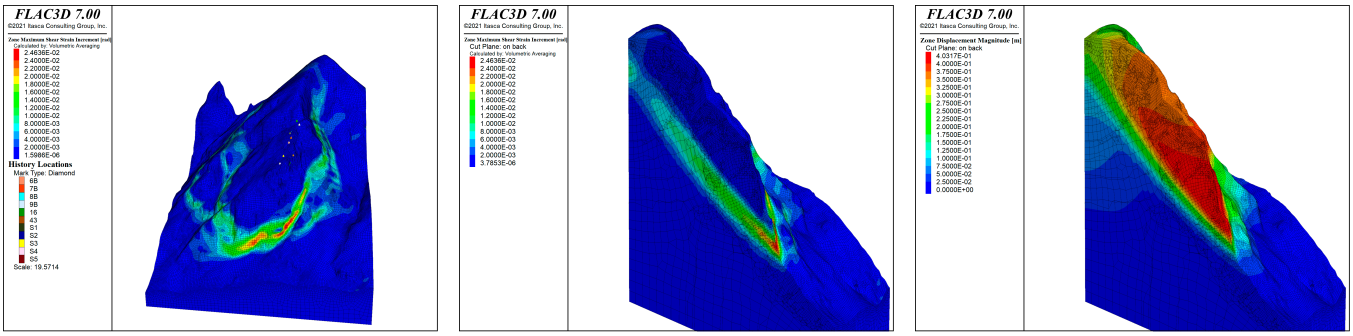

(**a**) (**b**) (**c**)

Figure 10. Model 1b 'after', F = 1.47: (**a**) contour plot of the shear strain increment; (**b**) section of the shear zone; and (**c**) section of the moving area (displacement magnitude).

Table 2 shows a comparison of the calculated reduction factors F_{stable} and $F_{unstable}$ of the two MC models 'Before' and 'After'.

Table 2. Calculated reduction factors for Model 1 MC.

Model 1 MC	F_{stable}	$F_{unstable}$
1a 'Before'	1.418	1.420
1b 'After'	1.470	1.473

With a safety factor of approximately 1.47, the 'After' model shows a higher overall stability than the 'Before' model with a safety factor of approximately 1.42. It can be concluded that the missing rock fall volume of approximately 117,000 m^3 (from the 2017 event) increases the overall stability of the 'After' model.

6.3. Model 2—Hoek–Brown

For model 2, the parameters are listed in Table 1 (column 'Initial Before and After'). The analysis of the valley flank is performed using the HB material model implemented in FLAC3D, with the listed HB parameters.

6.3.1. Model 2a—'Before'

For the terrain before the rock fall event 2017 (model geometry 'Before'), the reduction factor F_{stable} of the last stable state is 1.200. The reduction factor $F_{unstable}$ of the first unstable state is 1.207. The safety factor can thus be given as 1.20.

The reduction factor F cannot be applied to the original HB parameters (as discussed in Section 4).

We need to determine an HB material equivalent to the HB envelope at limit equilibrium state (i.e., reduced by F). This is achieved by adjusting the disturbance factor D (loosening factor). In this case, the GSI is not adjusted. The necessary disturbance factor D to approximate the limit equilibrium state is 0.37 (with a constant GSI of 34). The slope stability was analyzed with the resulting HB parameters listed in Table 1, in the column 'Limit Equilibrium Before'.

Figure 11 shows the envelopes for the in situ state (green), for the reduction with $F_{unstable}$ close to the limit equilibrium state (green-dot), and the envelope fitted by the disturbance factor D (yellow).

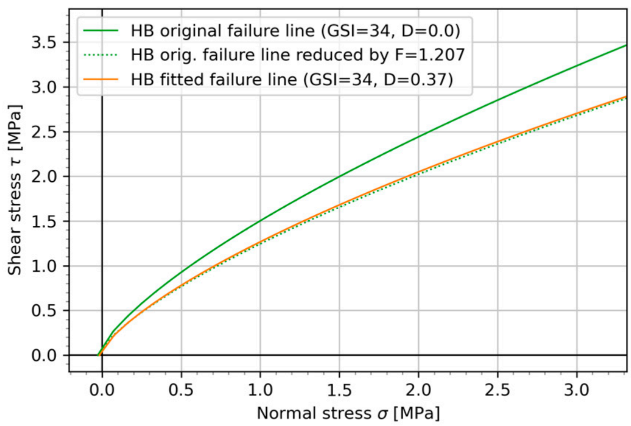

Figure 11. HB envelopes in the sigma-tau diagram for model 'Before'; green: failure envelope of the in situ state, green-dot: failure envelope of the limit equilibrium state (reduced by F = 1.207), and yellow: envelope fitted to the limit equilibrium state by D = 0.37.

Figure 12 shows the (a) contour plot of the shear strain increment, (b) the section of the shear zone, and (c) the section of the moving area (displacement magnitude). The volume of the calculated detachment (zones with velocities $\geq 1 \times 10^{-5}$ m/s) is 543,200 m^3 [19].

6.3.2. Model 2b—'After'

For the terrain after the rock fall event 2017 (model geometry 'After'), the reduction factor F_{stable} of the last stable state is 1.207. The reduction factor $F_{unstable}$ of the first unstable state is 1.211. The safety factor can thus be given as 1.21.

We need to determine an HB material equivalent to the HB envelope at limit equilibrium state (i.e., reduced by F). This is achieved by adjusting the disturbance factor D (loosening factor). In this case, the GSI is not adjusted. The necessary disturbance factor D to approximate the limit equilibrium state is 0.37 (with a constant GSI of 34). The slope stability is calculated with the resulting HB parameters listed in Table 1, in the column 'Limit Equilibrium After'.

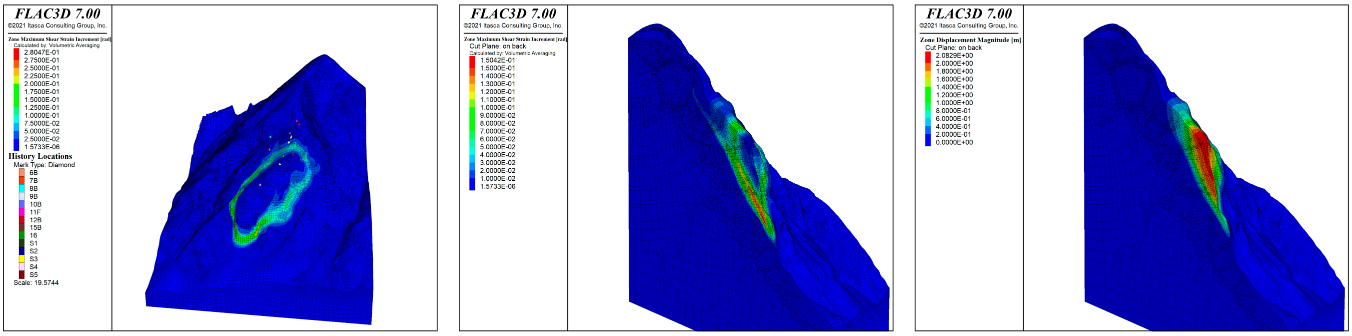

(**a**) (**b**) (**c**)

Figure 12. Model 2a 'Before', D = 0.37: (**a**) contour plot of the shear strain increment; (**b**) section of the shear zone; and (**c**) section of the moving area (displacement magnitude).

Figure 13 shows the envelopes for the in situ state (green), for the reduction with $F_{unstable}$ close to the limit equilibrium state (green-dot), and the envelope adjusted by the disturbance factor D (yellow).

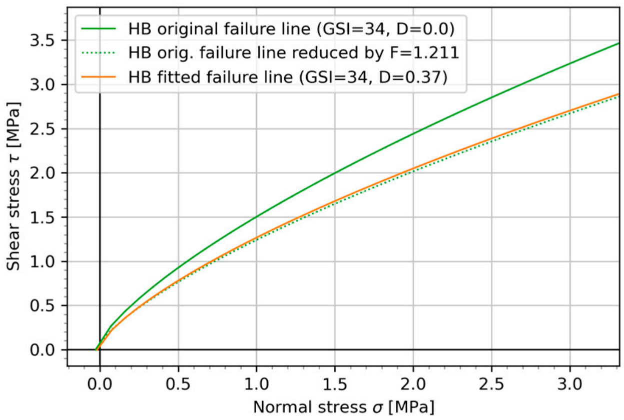

Figure 13. HB envelopes in sigma-tau diagram for model 'After'; green: failure envelope of the in situ state, green-dot: failure envelope of the limit equilibrium state (reduced by F = 1.211), and yellow: envelope fitted to the limit equilibrium state by D = 0.37.

Figure 14 shows the (a) contour plot of the shear strain increment, (b) the section of the shear zone, and (c) the section of the moving area (displacement magnitude). The volume of the calculated detachment^3 is 495,143 m^3 [19].

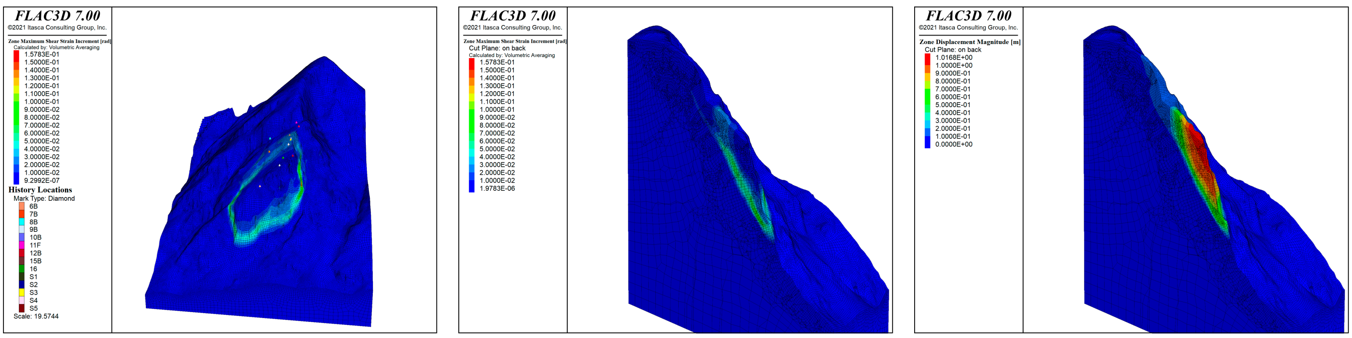

(**a**) (**b**) (**c**)

Figure 14. Model 2b 'After', D = 0.37: (**a**) contour plot of the shear strain increment; (**b**) section of the shear zone; and (**c**) section of the moving area (displacement magnitude).

6.3.3. Comparison of 'Before' and 'After' HB Model

A comparison of the calculated reduction factors F_{stable} and $F_{unstable}$ of the two HB models 'Before' and 'After' is shown in Table 3.

Table 3. Calculated reduction factors for model 2 Hoek–Brown.

Model 2 HB	F_{stable}	$F_{unstable}$
2a 'Before'	1.200	1.207
2b 'After'	1.207	1.211

The reduction factor $F_{unstable}$ of the 'Before' model is equal to the reduction factor F_{stable} of the 'After' model. This means that we can simulate that the safety of the slope is higher after the wedge of the 2017 event has broken off than before. However, the model cannot tell whether the predicted detachment volume will break off as a whole or in parts.

In both models, the displacements decrease with increasing depth (Figures 12c and 14c).

The volumes of the calculated detachments in the 'Before' and 'After' models are 543,200 m^3 and 495,143 m^3, respectively. This is a difference of 48,057 m^3. In the 'Before' model, the volume of the observed wedge failure of the 2017 event (117,000 m^3) is partly included in the calculated detachment volume. Both models show high concordance in terms of location and volume with the moving area identified by the TAC. To further adjust the model parameters, the model 'After' was calibrated.

6.4. Model Calibration

For model calibration, the moving area in the model was compared with the observation. A concordance check according to [15] was performed. The modeled and observed moving areas were projected onto the ground plane, superimposed, and compared. A displacement velocity of 1×10^{-5} m/s was set as the limit for the modeled unstable area [19].

The subarea of the superimposed modeled and observed moving areas (Figure 15) that overlap with one another is true positive (TP). The subarea outside of both the modeled and observed moving areas is true negative (TN). The modeled moving subarea that is outside the observed moving area is false positive (FP). The observed moving subarea that is outside of the modeled moving area is false negative (FN).

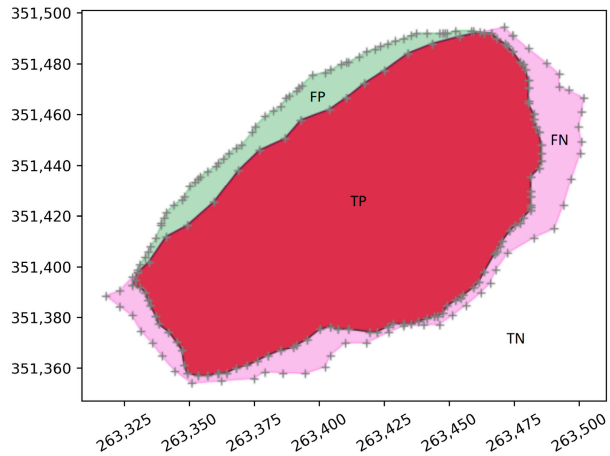

Figure 15. Concordance check by superimposing two areas projected onto the ground plane: the observed moving area (red and magenta) and modeled moving area (red and green; with HB parameters GSI = 34, m_i = 12, and D = 0.35); red: TP (modeled moving area matches observed moving area), green: FP (modeled moving area beyond observed moving area), and magenta: FN (observed moving area not represented in model).

From the thus determined subareas, the following values can be calculated:

- Critical success index (CSI);
- Heidke skill score (HSS);
- Distance to perfect classification (D2PC);
- Accuracy index (ACC).

The *CSI* indicates the percentage of positively correctly modeled areas of an observed region:

$$CSI = \frac{TP}{TP + FP + FN} \tag{19}$$

The *HSS* is used in the evaluation of meteorological forecasts and is an index for categorical forecasts [20]. The *HSS* can take values between $-\infty$ and 1, where 1 denotes the optimum:

$$HSS = \frac{2 \cdot (TP \cdot TN - FP \cdot FN)}{(TP + FP) \cdot (FP + TN) + (TP + FN) \cdot (FN + TN)} \tag{20}$$

The index *D2PC* is determined according to [15,21], where *TPR* is the true positive rate and *FPR* is the false positive rate. The *D2PC* takes values between 0 and 1. The optimum of this index is 0:

$$D2PC = \sqrt{(1 - TPR)^2 + FPR^2} = \sqrt{\left(1 - \frac{TP}{OP}\right)^2 + \left(\frac{FP}{ON}\right)^2}, \tag{21}$$

$$TPR = \frac{TP}{TP + FP} = \frac{TP}{OP}, \tag{22}$$

$$FPR = \frac{FP}{FP + TN} = \frac{FP}{ON}. \tag{23}$$

The *ACC* can assume values between 0 and 1, where 1 indicates the optimum of achieved accuracy. In contrast to *CSI*, the *ACC* takes the value of the true negative (*TN*) into account:

$$ACC = \frac{TP + TN}{TP + TN + FP + FN} \tag{24}$$

6.4.1. Calibration of the MC Model 'After'

We investigated the effect of different slope heights (using the SRM) in a study. The slope height was varied between 65 and 80 m. Another study investigated the effect of a variation of MC parameters (at limit equilibrium state). Cohesion and friction angles were varied between 0.24 MPa and 0.44 MPa, and between 31.1° and 32.6°.

Neither a variation of the slope height nor a variation of the MC parameters could improve the concordance of that modeled with the observed moving area.

6.4.2. Calibration of the HB Model 'After'

The results of the concordance check of the HB 'After' model are listed in Figure 16. A disturbance factor D of 0.35 and a GSI of 34 gives the highest concordance (i.e., 'best-fit') between the modeled and the observed moving areas (Figure 17).

6.5. Failure Prediction

With the result of the model calibration 'After', a predictive calculation of the moving area was performed. The HB parameters are listed in Table 1, in the column 'Limit Equilibrium After Best-Fit'.

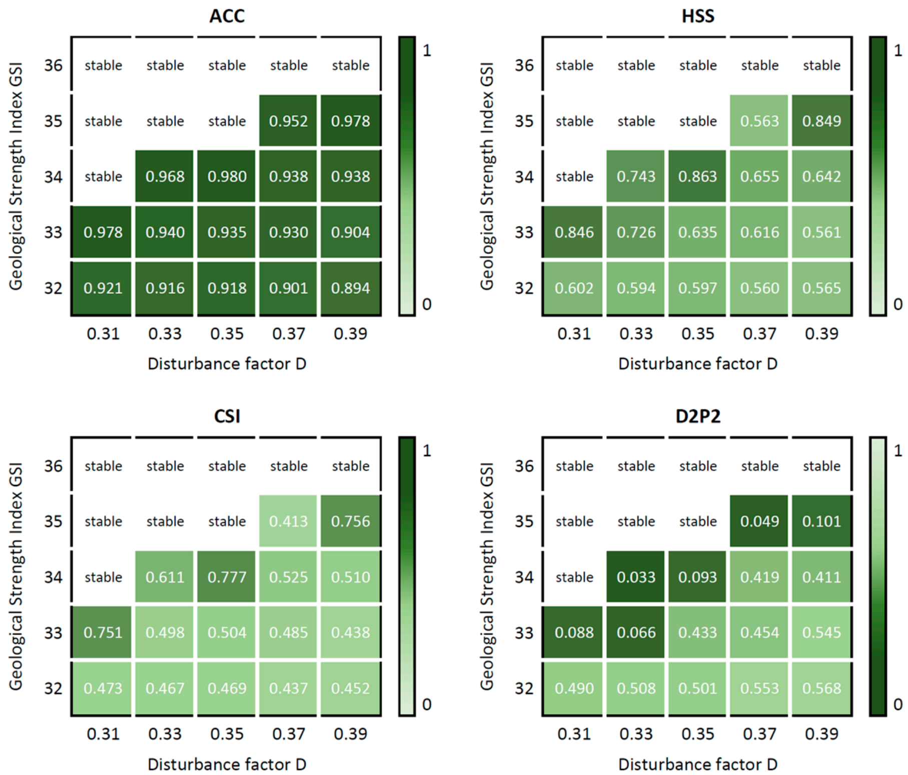

Figure 16. Results of the calibration model HB 'After'; dark green means best fit.

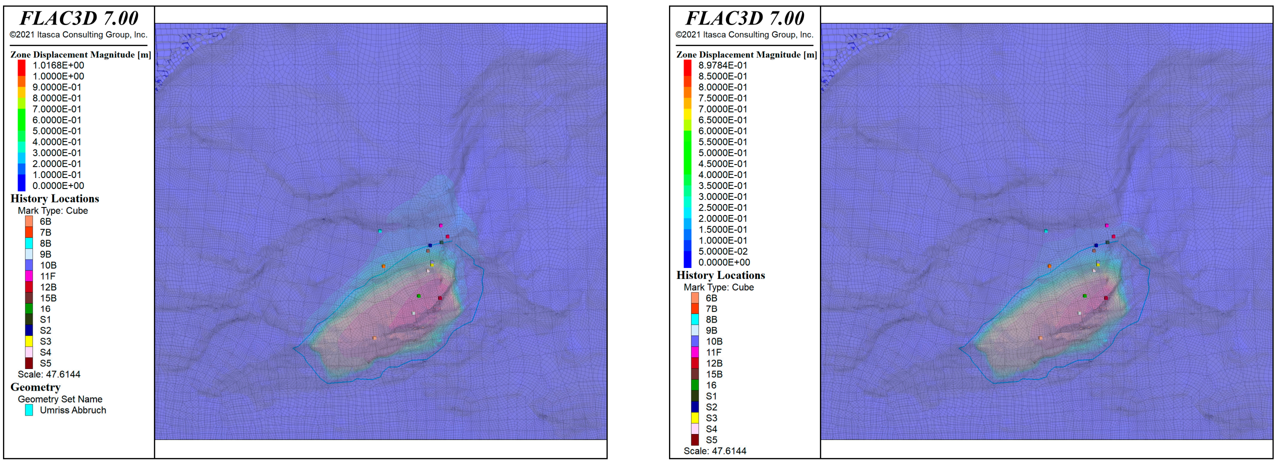

(**a**) (**b**)

Figure 17. HB model 'After': comparison of the moving areas (displacement magnitudes) with (**a**) D = 0.37 vs. (**b**) D = 0.35; cyan: outline of the observed moving area.

After the 2017 event (in July 2018), five extensometers (S1–S5) and 16 prisms were installed at the Vals valley flank and monitored. At the time of writing, the prisms show negligible displacements. Extensometers S1–S5 show more or less constant displacements between 1 mm (S3) and 10 mm (S2) per year. It can thus be concluded that the situation is stable. Currently, the safety factor is just above 1 or at 1.

The calibrated strength parameters were used to predict the displacements if the safety factor is just below 1. Figure 18a shows the contour plot of the shear strain increment. The unstable slope area (possible detachment) is limited by the shear band shown. It extends over the entire upper rock face from its base area to the observed tension crack (measuring points S1 and S2 in Figure 19a) at the top of the shear zone.

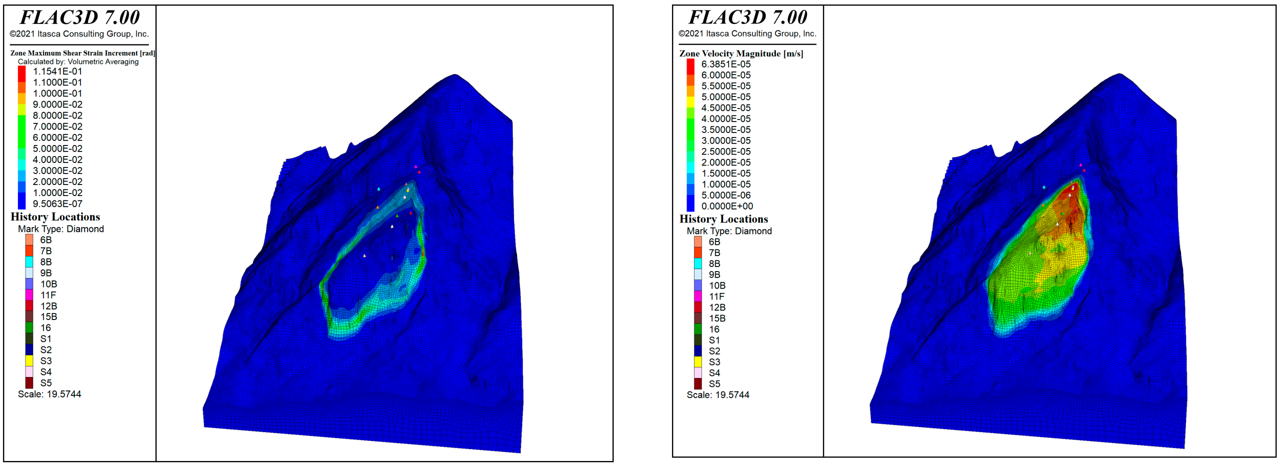

(**a**) (**b**)

Figure 18. Model 'Best-Fit', D = 0.35: (**a**) shear strain increment; and (**b**) displacement velocities.

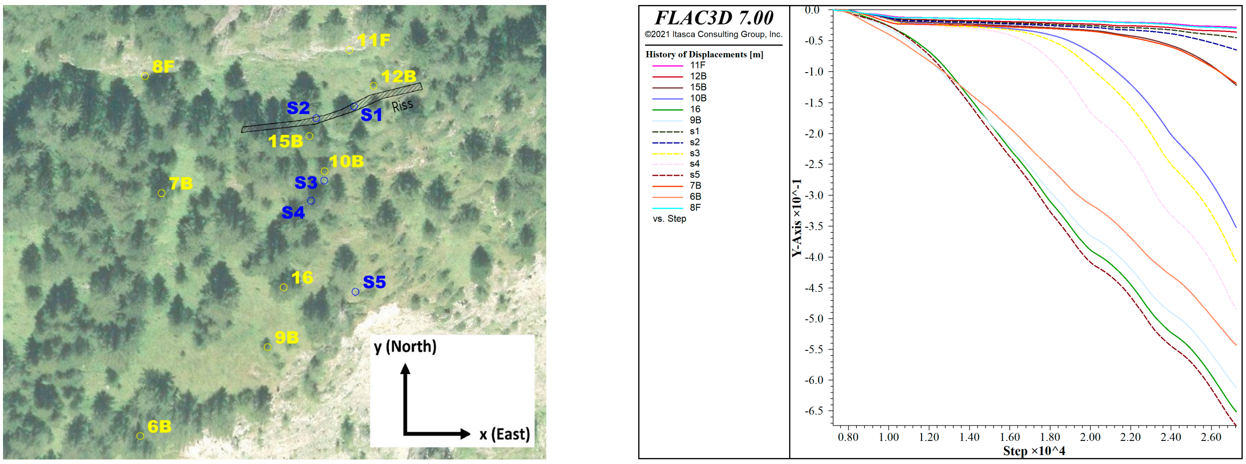

(**a**) (**b**)

Figure 19. Monitoring points: (**a**) overview of the actual monitoring points; (**b**) model 'Best-Fit', D = 0.35: course of the displacements [m] in negative y direction (i.e., towards South) over the calculation steps.

The displacements decrease with increasing depth (Figure 20b). The volume of the calculated detachment (zones with velocities $\geq 1 \times 10^{-5}$ m/s) is 411.277 m^3 [19].

Figure 19 shows the displacements of the monitoring points in the HB model 'Best-Fit'. Such calculations can only be used for qualitative predictions. The calculated records of displacements show that the monitoring points in the lower moving area (6B, 9B, 16, S5) start moving first. Later, displacements in the middle moving area (10B, S3, S4) increase. They accelerate relatively fast. Lastly, the monitoring points at the head of the moving area (especially around the observed tension crack (S1 and S2), 7B and 15B) show displacements. The displacement velocities in Figure 19b show that the monitoring points in the middle moving area (10B, S3, S4) accelerate the fastest at the end of the simulation. Note the steepest curves of these monitoring points. These findings can be used in the interpretation of the monitoring and may help in setting alert levels.

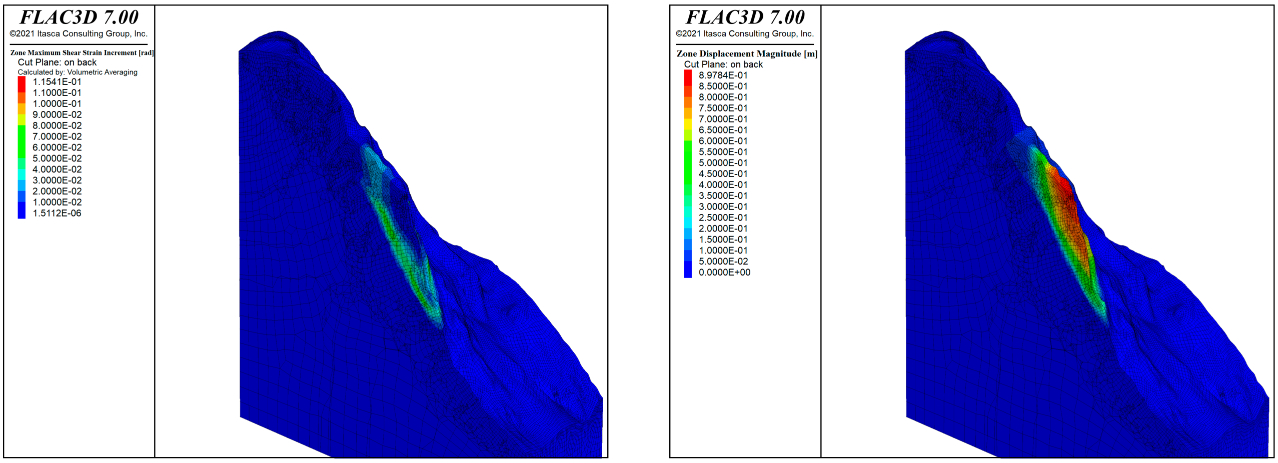

(**a**) (**b**)

Figure 20. Model 'Best-Fit', D = 0.35: (**a**) section of shear zone; and (**b**) section of moving region (displacement magnitude).

7. Discussion

The structural failure of the Vals valley flank in 2017 was a wedge failure. In such a case, the question arises whether a stability assessment using continuum mechanical (smeared) methods is expedient. From a geological point of view, the Vals rock mass is inhomogeneous and anisotropic. For this reason, a discontinuum mechanical calculation (DEM with 3DEC) was set up first. However, in the case in the Vals valley flank, a DEM calculation is not feasible or only feasible with strong simplifications. The extent and anisotropy of the rock face require an increase in joint spacings or a combination of joint orientations. On the larger scale, these heterogeneous and anisotropic conditions remain the same with depth. Thus, we can speak of 'homogeneous conditions' in slope scale. In continuum mechanical models, it is state of the art to describe heterogeneous rock masses such as flysch using the HB criterion [9]. We applied a GSI for the flyschoid sequence of the Vals rock mass in the range between 32 and 36.

According to [22] (p. 101ff), the effects of heavy blast damage as well as stress relief due to the removal of the overburden result in disturbance of the rock mass. The disturbance factor D was introduced to describe such stress relief effects in artificial slopes (and tunnels). It is considered that the disturbed rock mass properties using D = 1 are more appropriate for these 'artificial' rock masses. No blasting has been carried out on the Vals valley flank. We can assume that the former glacier melting and rock mass falls (including the event in 2017) led to stress relief and hence to some disturbance in the rock mass. Since the Vals valley flank is not an artificial slope, we consider initial rock mass properties using D = 0 as an appropriate baseline for the SRM. Hence, the calculated safety factors in Table 3 are with respect to the initial rock mass parameters with D = 0. We can assume that the Vals valley flank is near limit equilibrium.

The manipulation of both the GSI and D is plausible. It is more realistic to consider a range of the GSI rather than a single value. Additionally, we can assume that the rock mass was disturbed by prior slope movements and stress relief because of former glacier melting. GSI and D are also excellent for calibrating models, as demonstrated by the concordance check described in Section 6.4.

Displacement records cannot be directly implemented, because FLAC uses an attenuation where accelerations are damped (local damping). Thus, it is only possible to make qualitative displacement predictions.

In our discontinuum mechanical and continuum mechanical calculations, the models each consist of one homogeneous region (e.g., same joint spacing/material properties over the whole model). It was not possible to back-calculate the 2017 event with the homogeneous models. Thus, we can assume that it was caused by a local weak zone or a water-bearing layer within the rock mass. However, such conditions could not be mapped in the scarp area.

Our investigations show that a linear material model such as that of MC is poorly suited to represent both the brittle fracture behavior of rock at lower and ductile behavior at higher lateral stresses σ_3. The same problem exists when converting the HB parameters into equivalent MC parameters. Thus, a linear failure envelope is a poor approximation to the natural conditions. The HB criterion, with its curved failure envelope, is more appropriate. On the other hand, the HB criterion requires the determination of the GSI by field mapping. Additionally, the HB criterion is poorly suited for limit equilibrium studies because the SRM cannot be directly applied. In numerical models, this weakness is solved by introducing the apparent MC parameters. The challenge is to convert the apparent MC parameters back to HB parameters. The presented method shows a feasible way of doing this.

8. Conclusions

The presented method eliminates the difficulty of estimating a suitable range for smaller principal stresses (σ_3) via the 'slope height' (or 'tunnel depth').

For the present stability analysis with FLAC3D, it was not possible to back-calculate the structural wedge failure from 2017 using the HB criterion. However, it was possible to verify the currently most failure-prone area based on field mapping. However, this was not possible using equivalent MC parameters but only using apparent MC parameters. Using equivalent MC parameters results in a failure mechanism, which cannot be observed in nature, and in a higher safety factor!

Using equivalent MC parameters, it was also not possible to improve the concordance of the moving area between the model and observation by model calibration. This was tried with MC parameters equivalent to the HB parameters for different 'slope heights' and a variation of MC parameters. The present investigations clearly show that an application of equivalent MC parameters can lead to a wrong estimation of the overall stability. This was confirmed by [11].

The calibrated model may be used for qualitative displacement prediction. In this case, possible failure is not announced by displacements at the upper end of the moving area, near the observed tension crack. This is rather announced by displacements at the lower end of the moving area (6B, 9B, 16, S5). This information will enable targeted monitoring in the future.

Numerical methods provide reduction factors using the strength reduction method, which to date can only be applied to MC parameters but not to HB parameters. The presented method for calculating HB parameters from the chaotic distribution of apparent MC parameters by manipulating the GSI and D is a promising approach. This enables true limit equilibrium studies and prognostic calculations using the HB criterion with continuum mechanical numerical methods.

Author Contributions: Conceptualization, M.I. and A.P.; methodology, M.I. and A.P.; software, M.I. and A.P.; validation, M.I., A.P., and J.T.S.; formal analysis, M.I.; investigation, J.T.S. and A.P.; resources, J.T.S. and A.P.; data curation, A.P.; writing—original draft preparation, M.I., A.P., and J.T.S.; writing—review and editing, M.I., A.P., and J.T.S.; visualization, M.I. and J.T.S.; supervision, A.P.; project administration, M.I. and A.P. All authors have read and agreed to the published version of the manuscript.

Funding: Open Access Funding by TU Wien.

Institutional Review Board Statement: Not applicable.

Informed Consent Statement: Not applicable.

Data Availability Statement: The data presented in this study are available on request from the corresponding author. The data are not publicly available due to privacy restrictions.

Acknowledgments: We would like to thank the Galleria di Base del Brennero—Brenner Basistunnel BBT SE for the provision of existing laboratory test results [1]. The authors acknowledge Bibliothek for financial support through its Open Access Funding by TU Wien.

Conflicts of Interest: The authors declare no conflict of interest.

References

1. Materialversuchsanstalt_Strass. *Laborversuchsergebnisse BBT*; Pöyry Infra GmbH: Strass, Austria, 2014.
2. Dawson, E.M.; Roth, W.; Drescher, A. Slope stability analysis by strength reduction. *Geotechnique* **1999**, *49*, 835–840. [CrossRef]
3. Thiele, O. Das Tauernfenster. In *Der geologische Aufbau Österreichs*; Oberhauser, R., Ed.; Springer: Wien, Austria, 1980; pp. 300–314.
4. Frisch, W. Gradierte Serien am Tauernwestende—Zentralanstalt für Meteorologie und Geodynamik. *Geol. Tiefbau Ostalpen* **1978**, *230*, 23–24.
5. Schmid, S.M.; Scharf, A.; Handy, M.R.; Rosenberg, C.L. The Tauern Window (Eastern Alps, Austria): A new tectonic map, with cross-sections and a tectonometamorphic synthesis. *Swiss J. Geosci.* **2013**, *106*, 1–32. [CrossRef]
6. Frank, W.; Höck, V.; Miller, C. Metamorphic and tectonic history of the central Tauern Window. In *Geodynamics of the Eastern Alps*; Flügel, H.W., Faupl, P., Eds.; Deuticke: Vienna, Austria, 1987; pp. 34–54.
7. Staub, R. *Der Bau der Alpen. Beiträge zur Geologischen Karte der Schweiz*; Francke: Bern, Switzerland, 1924.
8. Fügenschuh, B.; Seward, D.; Mancktelow, N.S. Exhumation in a convergent orogen: The western Tauern Window. *Terra Nova* **1997**, *9*, 213–217. [CrossRef]
9. Marinos, P.; Hoek, E. GSI—A geologically friendly tool for rock mass strength estimation. In Proceedings of the GeoEng 2000, Melbourne, Australia, 19 November 2000; pp. 1422–1446.
10. Itasca. *FLAC3D: Fast Lagrangian Analysis of Continua in 3D, Version 7.0*; Itasca Consulting Group: Minneapolis, MN, USA, 2021.
11. Li, A.J.; Merifield, R.S.; Lyamin, A.V. Stability charts for rock slopes based on the Hoek–Brown failure criterion. *Int. J. Rock Mech. Min. Sci.* **2007**, *45*, 689–700. [CrossRef]
12. Hoek, E.; Carranza-Torres, C.; Corkum, B.C. Hoek-Brown criterion—2002 edition. In Proceedings of the 5th North American Rock Mechanics Symposium NARMS 2002, Toronto, ON, Canada, 7–10 July 2002; pp. 267–273.
13. Balmer, G. A general analytical solution for Mohr's envelope. *Am. Soc. Test. Mater.* **1952**, *52*, 1260–1271.
14. Hammah, R.; Yacoub, T.; Corkum, B.; Curran, J.H. The Shear Strength Reduction Method for the Generalized Hoek-Brown Criterion. In Proceedings of the Alaska Rocks 2005, The 40th US Rock Mechanics Symposium USRMS, OnePetro, Anchorage, AK, USA, 25–29 June 2005.
15. Mergili, M.; Fischer, J.-T.; Krenn, J.; Pudasaini, S.P. r. avaflow v1, an advanced open-source computational framework for the propagation and interaction of two-phase mass flows. *Geosci. Model Dev.* **2017**, *10*, 553–569. [CrossRef]
16. Rocscience. *RocData 5.011*; Rocscience Inc.: Toronto, ON, Canada, 21 September 2014.
17. Poisel, R.; Preh, A. Rock slope initial failure mechanisms and their mechanical models. *Felsbau* **2004**, *22*, 40–45.
18. Preh, A.; Illeditsch (former Zapletal), M. The perfect mesh for FLAC3D to analyze the stability of rock slopes. In Proceedings of the 4th International FLAC Symposium on Numerical Modeling in Geomechanics, Madrid, Spain, 29–31 May 2006; pp. 1–5.
19. Eccel, M. Comparison of the applicability of the Hoek-Brown and the Mohr-Coulomb failure criterion using the example of the Vals rock slope/Vergleich der Anwendbarkeit des Hoek-Brownschen und des Mohr-Coulombschen Bruchkriteriums am Beispiel der Felsböschung Vals. Master's Thesis, Vienna University of Technology, Vienna, Austria, 26 November 2021.
20. Hyvärinen, O. A Probabilistic Derivation of Heidke Skill Score. *Am. Meteorol. Soc. Weather Forecast.* **2014**, *29*, 177–181. [CrossRef]
21. Formetta, F.; Capparelli, G.; Versace, P. Evaluating performance of simplified physically based models for shallow landslide susceptibility. *Hydrol. Earth Syst. Sci.* **2016**, *20*, 4585–4603. [CrossRef]
22. Wyllie, D.C.; Mah, C.W. *Rock Slope Engineering, Civil and Mining*, 4th ed.; Taylor & Francis: New York, NY, USA, 2004.